Geophysical Research Letters

RESEARCH LETTER
10.1029/2019GL084258

Variations of Velocity and Attenuation Anisotropy Structures in the Uppermost Inner Core Beneath the Central Pacific Region

Jialing Qin[1,2], **Xinlei Sun**[1], **and An Fan**[1,2]

[1]State Key Laboratory of Isotope Geochemistry, Guangzhou Institute of Geochemistry, Chinese Academy of Sciences, Guangzhou, China, [2]University of Chinese Academy of Sciences, Beijing, China

Key Points:
- Both velocity and attenuation anisotropy in the uppermost 100 km of the inner core beneath the central Pacific are investigated
- We find clear variations in both velocity and attenuation anisotropy structures, and there exist good correlation between them
- The inner core growth may be coupled with core-mantle boundary heterogeneity and different deformation processes

Supporting Information:
- Supporting Information S1

Correspondence to:
X. Sun,
xsun@gig.ac.cn

Citation:
Qin, J., Sun, X., & Fan, A. (2019). Variations of velocity and attenuation anisotropy structures in the uppermost inner core beneath the central Pacific region. *Geophysical Research Letters*, *46*, 11,811–11,819. https://doi.org/10.1029/2019GL084258

Received 26 JUN 2019
Accepted 5 OCT 2019
Published online 6 NOV 2019

Abstract Using PKIKP and PKiKP travel times and amplitude ratios, we examine the velocity and attenuation anisotropy structures in the uppermost 100 km of the inner core beneath the central Pacific region. Our results indicate a clear change from approximately 180°E to 190°E longitude. Below the western Pacific, velocity anisotropy is weak and attenuation is high (Qp ~200), whereas below the eastern Pacific, velocity anisotropy is strong (3.3%) and attenuation is low (Qp ranges from 400 to 150). Furthermore, the velocity and attenuation anisotropies are correlated with each other. Our results indicate that the growth of the inner core may be coupled with core mantle boundary thermal heterogeneities. The heterogeneities may affect directional heat flow or deformational processes in the uppermost inner core, cause different iron crystal alignments, and result in lateral variations in anisotropy structures.

Plain Language Summary The inner core solidified from the liquid outer core, so the structure at the top inner core is closely linked to its formation process. In this study, based on seismic data availability, we choose the uppermost 100 km of the inner core beneath the Pacific region and investigate in detail its velocity and attenuation differences in different directions, or anisotropy structures. Our results not only depict a transition boundary between the eastern and western Pacific but also show different anisotropy characteristics of these two regions, in which the western/eastern Pacific region shows weak/strong anisotropy in both velocity and attenuation. Moreover, the velocity and attenuation anisotropies are correlated. These results indicate that the inner core growth may be coupled with the core mantle boundary heterogeneity, which may cause different texture alignment through different deformation or heat flow, and result in different physical properties in the inner core.

1. Introduction

As the Earth cools, the inner core grows through gradual solidification of the liquid outer core (Jacobs, 1953). During this solidification, latent heat is released, and light elements are expelled into the outer core. These processes drive the thermochemical convection of the outer core, generate the Earth's magnetic field, and are important to maintain the Earth's geodynamo (Fearn & Loper, 1981; Gubbins, 1977; Loper, 1978). The velocity and attenuation structures of the uppermost inner core may preserve signatures of this cooling process and provide important constraints on the inner core's growth.

Previous seismological studies have demonstrated complex structures in the uppermost inner core and suggested that the *P* wave velocity and attenuation in the upper 100 km of the inner core exhibit hemispherical variations (Cao & Romanowicz, 2004; Niu & Wen, 2001; Waszek & Deuss, 2011; Yu & Wen, 2006a). In the eastern hemisphere, the *P* wave velocity and attenuation are high whereas in the western hemisphere, the *P* wave velocity and attenuation are low. Furthermore, recent studies revealed velocity and attenuation heterogeneities within the same hemisphere to at least 300 km below the inner core boundary (ICB; Iritani et al., 2014; Stroujkova & Cormier, 2004; Tanaka, 2012), and the correlation of fast/slow velocity and high/low attenuation changes underneath the Pacific region (which is in the western hemisphere) in the inner core (Attanayake et al., 2014). A recent global attenuation tomography model in the top 400 km of the inner core also revealed complicated heterogeneities (Pejić et al., 2017). These results suggested that the structures in the uppermost inner core are more complex than hemispherical variations. However, due to the limited ray path coverage, particularly along the north-south directions, studies of the anisotropy in the top 100 km of the inner core are scarce (Yu & Wen, 2007).

Two mechanisms have been proposed to explain the hemispherical variations of the uppermost inner core structure. The first mechanism involves the convective translation of the inner core (Alboussiere et al., 2010; Monnereau et al., 2010), which predicts melting/freezing in the eastern/western hemispheres. The second mechanism involves coupling between the inner core growth and the core mantle boundary (CMB) heat flux (Aubert et al., 2008; Gubbins et al., 2011). It also predicts melting and freezing in the inner core, but in opposite locations compared to the first mechanism. Although these mechanisms can explain the isotropic hemispherical structures in the uppermost inner core, they cannot explain the heterogeneities within the same hemisphere or the anisotropy at different depths in the inner core. Thus, other mechanisms need to be considered.

In this study, we investigate the *P* wave velocity and attenuation anisotropy structures in the uppermost inner core beneath the central Pacific. Lateral variations, as well as relationships between the velocity and attenuation anisotropy structures, are investigated. Such detailed research in the inner core is relatively uncommon and can better constrain the mechanism of the inner core growth.

2. Data and Method

The data we use are PKIKP and PKiKP phases, which travel through the inner core and are reflected back from the ICB, respectively (Figure 1a). All the data are requested from the IRIS DMC. The earthquakes we select have magnitude (Mw) greater than 5.5 and reported focal depths greater than 15 km. The epicentral distances of seismograms range from 130° to 142°, and the turning points of the PKIKP ray paths are between the longitudes 160°E to 240°E and the latitudes 30°S to 30°N. The time period of the data spans from 2000 to 2017.

All seismograms are deconvolved with the instrument response and band pass filtered between 0.5 and 1.5 Hz. We visually check the data to select the good quality ones. During this process, seismograms from the same earthquake are aligned according to their distances, which makes it easy to trace the target phases. We select only the seismograms that have good signal to noise ratio and clear separation of PKIKP and PKiKP, as well as their surface reflections. Finally, a total of 577 seismograms for 134 events are chosen. Example seismograms are shown in Figure 1b.

In this paper, we define the ray angle (ξ) as the angle between the PKIKP ray path in the inner core and the north-south direction. Ray paths with $\xi > 40°$ are defined as equatorial paths; otherwise, they are defined as polar paths.

The amplitude ratios and differential travel times of PKIKP and PKiKP are measured based on the relative peak-to-trough magnitudes and time separations of these two phases (Figure 1b). Residuals of PKiKP-PKIKP differential travel times are calculated using PREM (Dziewonski & Anderson, 1981) and are corrected for the mantle structure based on the MIT *P* wave tomographic model (Li et al., 2008).

The PKIKP and PKiKP travel time residuals and amplitude ratios (Figures 1c and 1d) show clear variations with longitude (Figures 1, S1, and S2 in the supporting information). Toward the east, the residuals decrease for equatorial data and increase for polar data, while the amplitude ratios increase for equatorial data but decrease for polar data. The transition boundaries for the travel times and amplitude ratios all lie between approximately 180°E to 190°E longitude and are plotted using red dashed lines in Figures 1c and 1d. Because we do not have sufficient data at middle latitudes, we use black dotted lines to represent the boundary.

We divide the Pacific region into two subregions, the western Pacific and eastern Pacific, which lie to the west and east, respectively, of approximately 180°E longitude. The western and eastern Pacific regions belong to the eastern and western hemispheres of the inner core, respectively. We invert the velocity anisotropy and attenuation anisotropy in these two regions separately.

Following Sun and Song (2008), the velocity anisotropy is expressed as

$$\frac{\delta t}{t} = \frac{\delta v}{v} = \alpha + \varepsilon \cos^2 \xi + \gamma \sin^2 2\xi, \tag{1}$$

where δt is the PKiKP-PKIKP travel time residuals, t is the travel time of PKIKP in the inner core, ξ is the ray angle of PKIKP, α is the velocity perturbation in the equatorial plane, ε is the amplitude of anisotropy, and γ

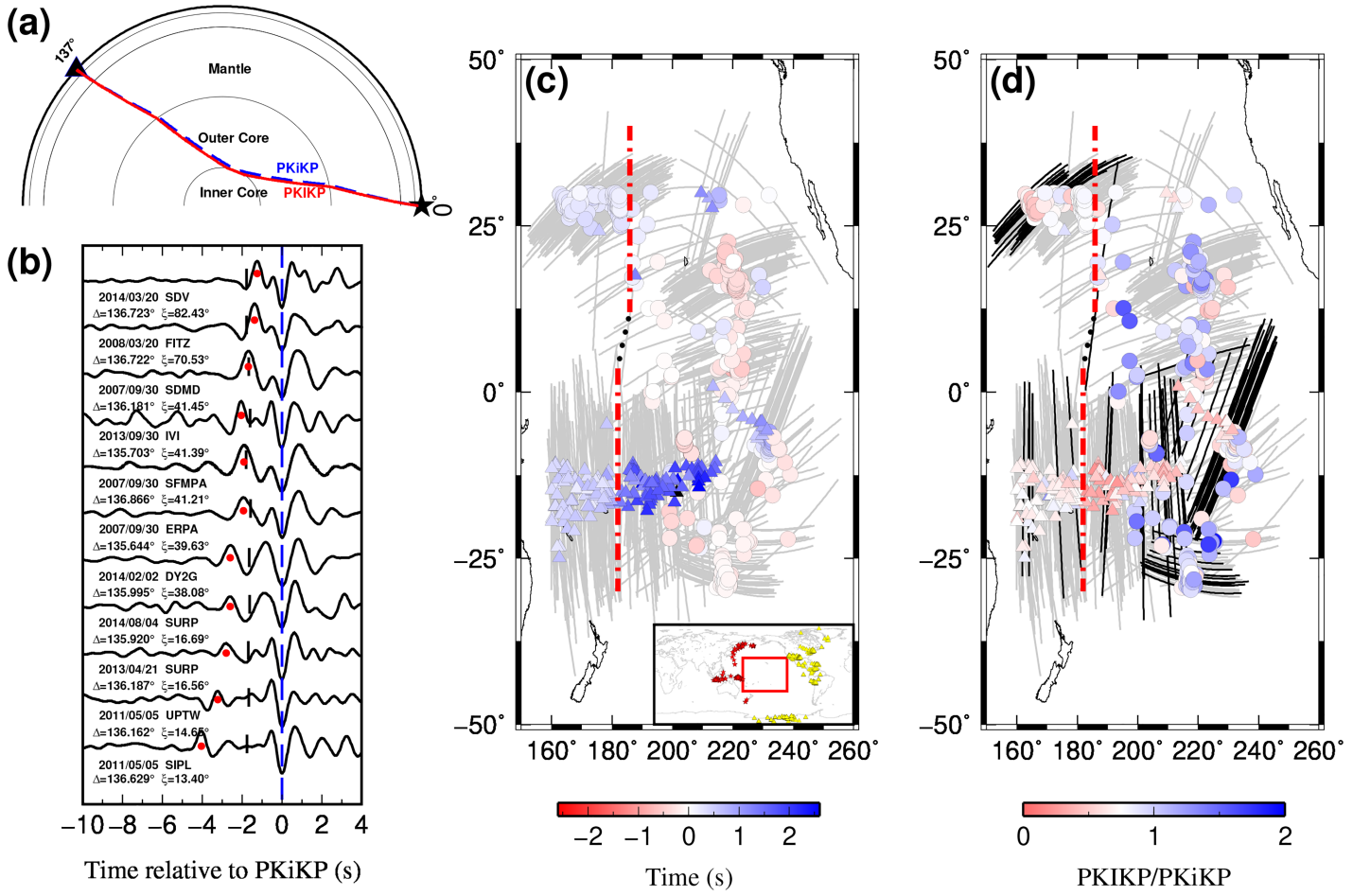

Figure 1. PKIKP and PKiKP data used in this study. (a) Ray paths of PKIKP (red solid) and PKiKP (blue dashed) at an epicentral distance of 137°. The star denotes an earthquake at 100 km depth and the triangle denotes a seismic station. (b) Example PKIKP and PKiKP waveforms. All waveforms are aligned with PKiKP, and the observed PKIKP are indicated with red dots, while the predictions are indicated using short black solid lines. The station name, epicentral distance and ray angle, as well as the earthquake information are listed on the left side of each seismogram. (c) Map view of the PKiKP-PKIKP differential travel time residuals. Gray solid lines denote PKIKP ray paths through the inner core, while circles and triangles correspond to the turning points of PKIKP for equatorial and polar paths, respectively. The boundary between different residuals is plotted using dashed line. The inserted map shows the locations of the earthquakes (stars) and stations (triangles) used in this study. (d) Same as (c) but for the amplitude ratios of PKIKP/PKiKP. Among them, the black lines represent the ray paths of our modeled seismograms in Figure 4.

contributes to anisotropy at intermediate angles. Because the ray path changes as the velocity model changes, we invert the velocity anisotropy iteratively. Before each inversion, the velocity model is updated for each ray path according to the results of the previous inversion.

The Q value (Q refers to Qp throughout our text) inversion follows the procedure of Tanaka (2012), which is calculated based on observed and synthetic PKIKP/PKiKP amplitude ratios using the following equations:

$$\frac{\left(A_{PKIKP/PKiKP}\right)_{obs}}{\left(A_{PKIKP/PKiKP}\right)_{syn}} = \exp\left(-\pi f dt^*\right) \quad dt^* = t^*_{obs} - t^*_{syn} \quad t^* = t_{IC}/Q_{IC}, \tag{2}$$

where A is the amplitude, f is the dominant frequency, t^* is the integration of the travel time t over the quality factor Q, dt^* is the difference between the observed (t^*_{obs}) and synthetic data $\left(t^*_{syn}\right)$, t_{IC} is the P wave travel time in the inner core, and Q_{IC} is the P wave quality factor in the inner core.

It is worth noting that when we calculate the attenuation, instead of using a 1-D reference model, we use different velocity models for different rays. Using our anisotropic velocity inversion results, we generate velocity models with a 1° interval from equatorial to polar directions and then use the velocity model in each ray's

nearest direction to synthesize its PKIKP and PKiKP waveforms. The starting value of Q is 240, and the synthetic seismograms are computed using the direct solution method (Kawai et al., 2006).

3. Results

3.1. Velocity and Attenuation Anisotropy Models of the Two Regions

Figure 2 shows the velocity anisotropy models of the first and the final inversions for the eastern and western Pacific regions. Since the velocity anisotropy in the western Pacific is small (~0.5%), the inversion results from different iterations are very similar. However, in the eastern Pacific region, the anisotropy amplitude changes from 4.4% to 3.3%, because PKIKP ray paths transverse greater depths in the anisotropic velocity models.

The anisotropy coefficients of the eastern and western Pacific regions can be found in Table S1. Figure S3 displays examples of the calculated anisotropic velocity models at different ray angles in the western and eastern Pacific.

The inverted Q values in the two Pacific regions are summarized in Figure 3. We average the data using 10° windows, with a moving step of 5°. The attenuation in the eastern Pacific region exhibits a strong anisotropy, with an increase in attenuation from equatorial (Q ~400) to polar directions (Q ~150). In contrast, the attenuation values in the western Pacific are very similar in all directions (Q ~200), suggesting weak anisotropy. Figure S4 displays a 3-D view of the attenuation distribution throughout the central Pacific. Longitudinal and directional changes are clearly shown.

Figure 4 shows the observed and synthetic waveforms in different regions and different directions. All data fit pretty well, although the waveforms in polar directions in the eastern Pacific region display some misfit at smaller distances. This indicates that uniform anisotropy models in the uppermost 100 km of the inner core may not be accurate, and further exploration of anisotropy depth variations is required if data coverage is adequate in all directions.

3.2. Velocity and Attenuation Correlation

Our results show a clear correlation between the velocity and attenuation anisotropies in the Pacific region (Figure 5). The velocity perturbations and attenuations are binned every 10° according to the PKIKP ray angles, with a moving step of 5°. In the equatorial directions (open symbols), the western Pacific shows fast velocity and high attenuation, while the eastern Pacific displays slow velocity and low attenuation. In the polar directions, especially in the eastern Pacific region, this velocity and attenuation correlation persists (solid symbols). On the other hand, the attenuation anisotropy shows an obvious correlation with the velocity anisotropy, that is, strong/weak velocity anisotropy correlates with strong/weak attenuation anisotropy.

The positive correlation between velocity and attenuation in the equatorial directions has been previously reported at very large scales (Wen & Niu, 2002; Yu & Wen, 2006b). However, inconsistency of this relation at regional scales has been observed (Attanayake et al., 2014). Nevertheless, on an even smaller scale in the central Pacific, our results show a positive correlation between velocity and attenuation in both the equatorial and polar directions, which is consistent with previous studies in large scales (Souriau & Romanowicz, 1996; Yu & Wen, 2006a).

4. Discussion

Mantle effects are also corrected in this study, although they are relatively negligible because the PKIKP and PKiKP ray paths are so close (Figure S5). In fact, the inner core velocity model is far more important in inverting the velocity anisotropy and attenuation, as it can change the ray paths and amplitudes of PKP phases greatly.

4.1. Comparison with Previous Studies

We summarize various velocity and attenuation results in the uppermost 100 km of the inner core in Table S2.

In the equatorial directions, our velocity and attenuation results are generally consistent with those of previous studies from both hemispherical and regional perspective. On the other hand, our results reveal strong (3.3%) velocity anisotropy and obvious attenuation anisotropy in the eastern Pacific, whereas some

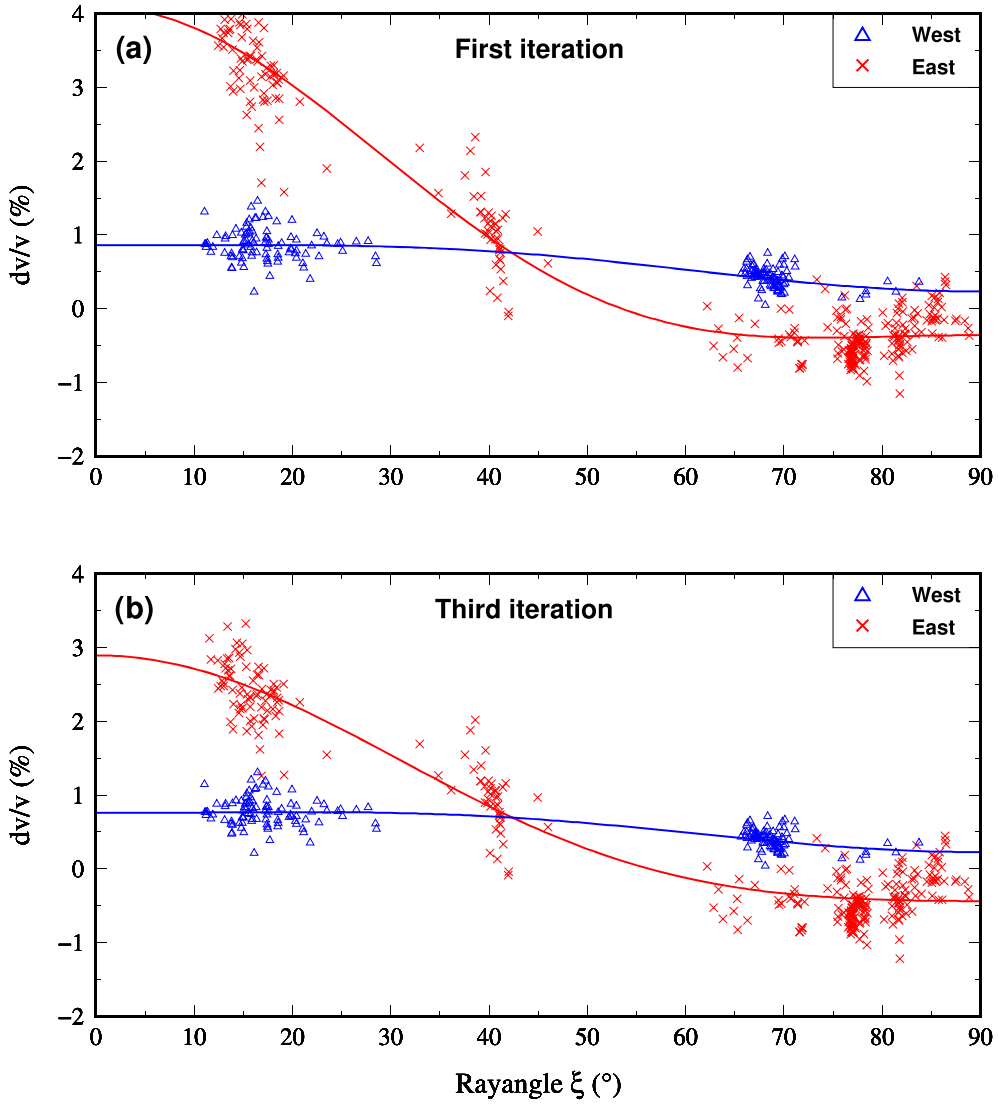

Figure 2. Inner core velocity perturbations as a function of the ray angles sampling the western (blue triangles) and eastern (red crosses) Pacific regions. Solid lines are the predictions of the anisotropy model. (a) and (b) are the inversions based on the 1-D PREM model and updated anisotropic velocity model, respectively.

previous studies indicate that the top 100 km of the inner core has isotropic or weakly anisotropic structure (Cao & Romanowicz, 2004; Niu & Wen, 2001; Wen & Niu, 2002; Yu & Wen, 2006a). Nevertheless, anisotropy has been discovered in the top inner core in some other regions. For example, complex velocity and attenuation anisotropies were reported in the uppermost inner core beneath the Africa (Yu & Wen, 2007), and Waszek and Deuss (2011) inverted 2.8% velocity anisotropy in the western hemisphere. Although there are some differences in the anisotropy structures, these results generally agree that the uppermost inner core has high attenuation and fast velocity in the polar direction and low attenuation and slow velocity in the equatorial direction.

More recently, Waszek and Deuss (2013) suggested that the attenuation anisotropy of the uppermost inner core can be explained by an anisotropic velocity model, as the velocity jump across the ICB at different directions will affect the amplitudes of both PKIKP and PKiKP and thus change their amplitude ratios in the polar and equatorial directions. Accordingly, we test different velocity models (0–3% anisotropy) in the inner core and find that the anisotropic velocity models can change the amplitude ratios of PKIKP/PKiKP of up to 0.2 (Figure S6). Since we have considered this effect in our inversion, both our velocity and attenuation anisotropy structures are reliable.

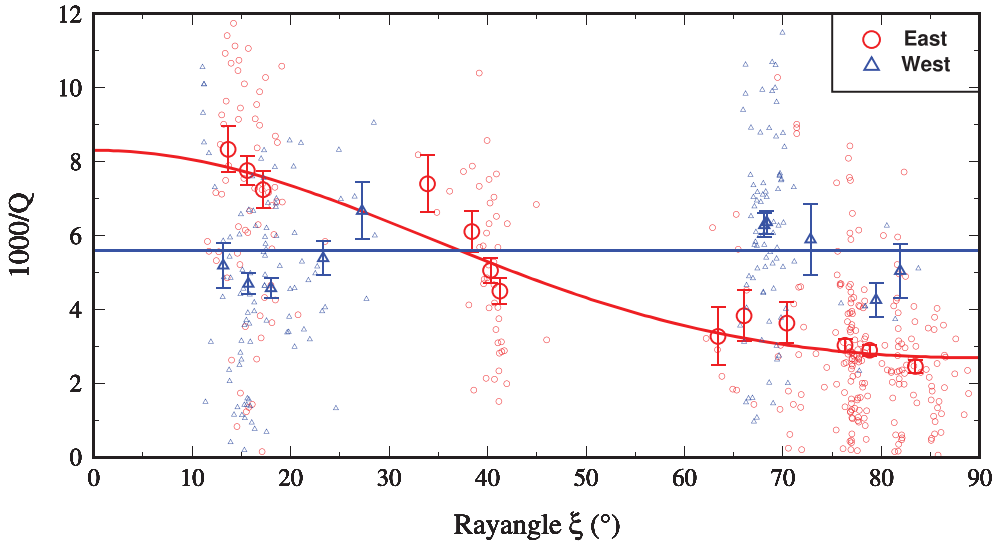

Figure 3. Attenuation for the eastern (red symbols) and western (blue symbols) Pacific regions in different directions. The error bar denotes one standard deviation.

One boundary between the western and eastern hemispheres of the inner core is believed to be beneath the Pacific region between 160°E and 180°E longitude. Using velocity variations, Yu et al. (2017) found a kink in the boundary between these two hemispheres. Our study region overlaps the northern part of their study, and our results are consistent with the rough position of this boundary. Waszek and Deuss (2011) also investigated this boundary by dividing the equatorial PKiKP-PKIKP data into different distance groups. They concluded that this boundary lies between 187°E to 200°E longitude and shifts eastward with increasing depth. In our study, we treat the uppermost 100 km of the inner core as a uniform layer, so our results do not have depth resolution. Nevertheless, these results are all generally consistent with each other, suggesting that the position of this boundary is reliable. However, due to the limited sampling of the inner core, it is not easy to distinguish whether this boundary constitutes a hemispherical division or represents only a local boundary.

The uppermost 100 km of the inner core may have a very complex structures in both velocity and attenuation structures. Therefore, caution must be taken when studying the deeper structure of the inner core using PKPBC and PKIKP phases. Combining PKiKP-PKIKP and PKPBC-PKIKP data to investigate how the velocity and attenuation anisotropies change with depth would be helpful in future studies.

4.2. Mechanism for the Uppermost Inner Core Structure

Many studies have focused on the mechanisms that can explain the hemispherical variations of the uppermost inner core structure. These mechanisms generally involve freezing and melting in different regions of the inner core (Alboussiere et al., 2010; Aubert et al., 2008; Gubbins et al., 2011; Monnereau et al., 2010). However, these models have difficulties in explaining the nonhemispherical structures and the strong velocity and attenuation anisotropies in the uppermost inner core, as revealed in our study and some other studies. In order to explain the inner core anisotropy, the variations, and the correlation between the velocity and attenuation, alternative mechanisms should be considered.

The velocity and attenuation anisotropies of the inner core are generally believed to be caused by the lattice preferred orientation or preferred alignments of iron crystals in the inner core. To explain the preferred alignments of these iron crystals, various processes have been proposed, such as solid-state convection (Jeanloz & Wenk, 1988), texture alignment resulting from the tangential Maxwell stress (Buffett & Wenk, 2001), and magnetic stress from the outer core convection (Karato, 1999). Bergman (1997) pointed out that the preferred solidification texture of iron crystals can be achieved in a preferred direction of heat extraction. This process can explain not only the velocity anisotropy but also the attenuation dependence of the directions by the number of crystal boundaries seismic waves transverse. Another mechanism arises from different deformation of the iron crystals attributed to different stresses (Reaman et al., 2011). In this hypothesis, small iron

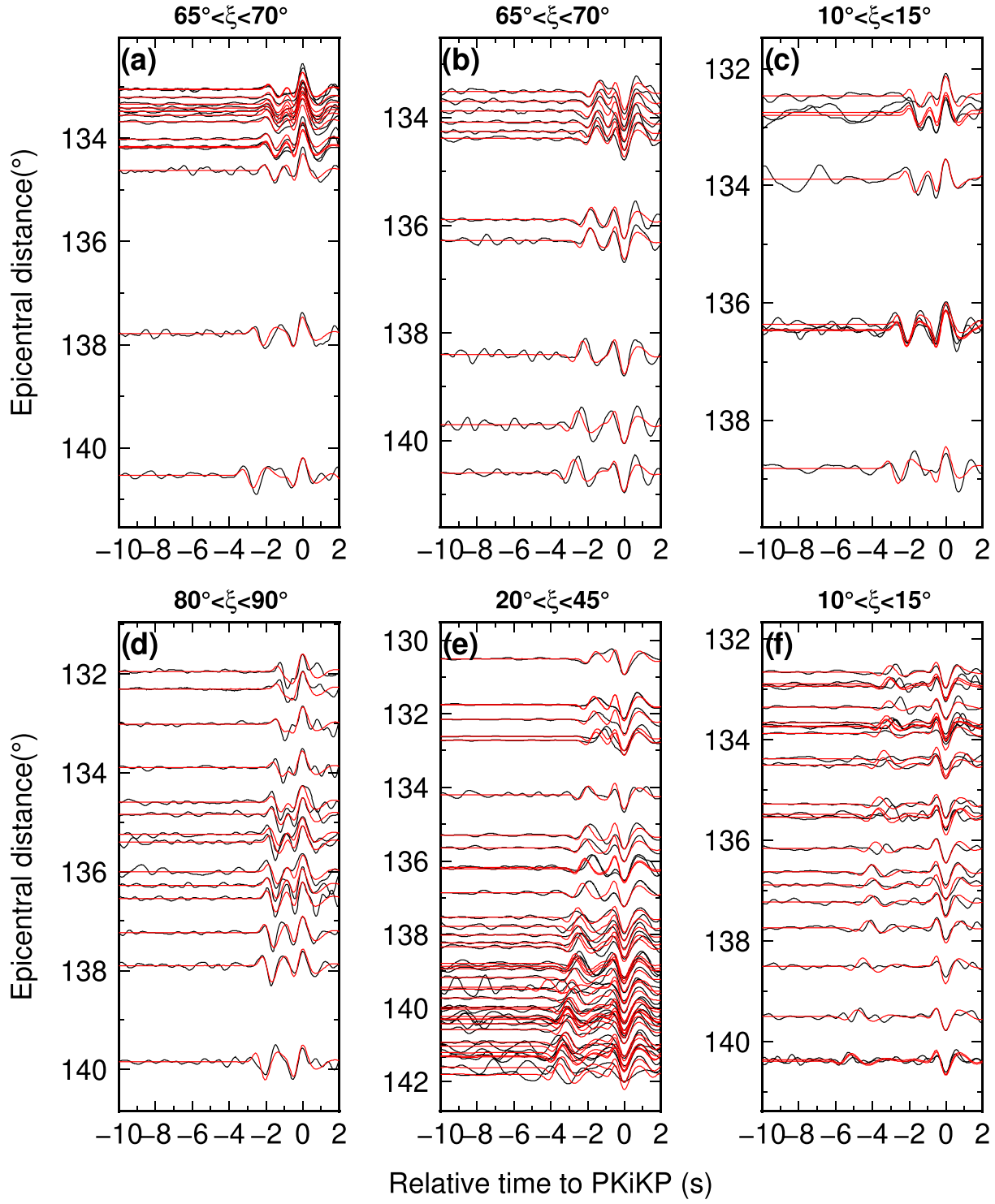

Figure 4. Comparison between the observed (black lines) and synthetic (red lines) waveforms in the eastern and western Pacific regions in different directions. The traces are aligned with PKiKP. (a)–(c) and (d)–(f) are for waveforms sampling the western and eastern Pacific, respectively. The ray angles of these seismograms are labeled at the top of each panel.

crystals controlled by diffusion creep deformation are randomly oriented and thus show weak/no anisotropy. However, when the crystals grow larger, the dominant deformation changes to dislocation creep, which allows the development of preferred iron crystal alignment or the occurrence of anisotropy. If the stresses

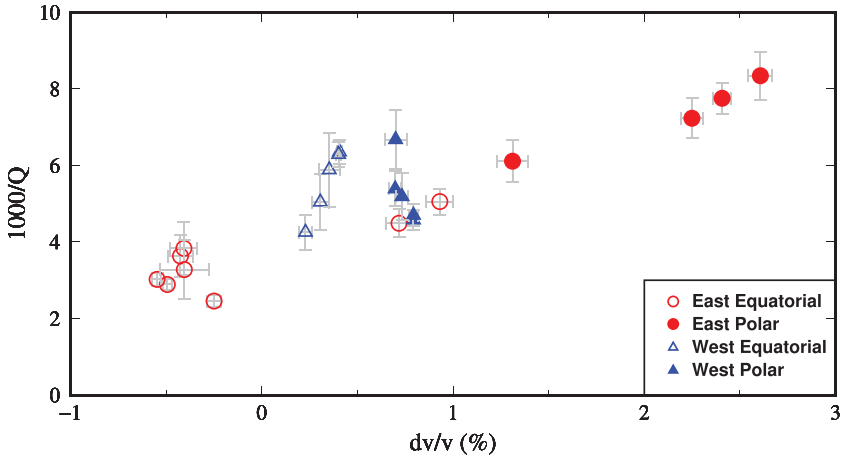

Figure 5. Correlations between the attenuation and velocity anisotropies in the study area. Red circles and blue triangles signify averaged data for the eastern and western Pacific, respectively, and open and solid symbols are for equatorial and polar data, respectively. The error bar denotes one standard deviation.

in various areas of the inner core are different, then the iron crystals may be dominated by different deformation processes and show distinctive anisotropy characteristics. If processes such as these are coupled with CMB thermal heterogeneities, then these processes can likely explain the hemispherical/local variations in the uppermost inner core structure.

Finally, we must note that although the translation model can explain the sharp boundary between the hemispheres of the inner core (Geballe et al., 2013), it is not impossible that variations in heat flux or deformation patterns could also have a similar effect.

5. Conclusions

By analyzing PKiKP-PKIKP differential travel time residuals and PKIKP/PKiKP amplitude ratios, we invert both the velocity and attenuation anisotropies in the uppermost 100 km of the inner core beneath the central Pacific region. We find that the western and eastern Pacific regions, separated by a boundary between 180°E and 190°E longitude, show very different characteristics. The western Pacific demonstrates weak velocity and attenuation anisotropies, whereas the eastern Pacific shows strong velocity anisotropy (3.3%) and obvious attenuation anisotropy (the Q value changes from 400 to 150 from equatorial to polar directions). Moreover, the velocity and attenuation show a positive correlation in the equatorial and polar directions. These results may be related to regional variations in the inner core solidification or deformation processes. It is likely that these processes are coupled with CMB thermal heterogeneities and finally cause different alignment of the iron crystals in the inner core.

Acknowledgments
We thank Jeroen Ritsema, the Associate Editor, V.F. Cormier, and two anonymous reviewers for their constructive comments and suggestions. This research is supported by National Science Foundation of China (NSFC 41774053, 41330209, and 41274057) and the Strategic Priority Research Program (B) of Chinese Academy of Sciences (Grant XDB18000000). The facilities of IRIS Data Services, and specifically the IRIS Data Management Center (https://www.iris.edu/hq/), were used for access to waveforms, related metadata, and/or derived products used in this study. IRIS Data Services are funded through the Seismological Facilities for the Advancement of Geoscience and EarthScope (SAGE) Proposal of the National Science Foundation under Cooperative Agreement EAR-1261681.

References

Alboussiere, T., Deguen, R., & Melzani, M. (2010). Melting-induced stratification above the Earth's inner core due to convective translation. *Nature*, *466*(7307), 744–747. https://doi.org/10.1038/nature09257

Attanayake, J., Cormier, V. F., & de Silva, S. M. (2014). Uppermost inner core seismic structure: New insights from body waveform inversion. *Earth and Planetary Science Letters*, *385*, 49–58. https://doi.org/10.1016/j.epsl.2013.10.025

Aubert, J., Amit, H., Hulot, G., & Olson, P. (2008). Thermochemical flows couple the Earth's inner core growth to mantle heterogeneity. *Nature*, *454*(7205), 758–761. https://doi.org/10.1038/nature07109

Bergman, M. I. (1997). Measurements of elastic anisotropy due to solidification texturing and the implications for the Earth's inner core. *Nature*, *389*(6646), 60–63. https://doi.org/10.1038/37962

Buffett, B. A., & Wenk, H. R. (2001). Texturing of the Earth's inner core by Maxwell stresses. *Nature*, *413*(6851), 60–63. https://doi.org/10.1038/35092543

Cao, A., & Romanowicz, B. (2004). Hemispherical transition of seismic attenuation at the top of the Earth's inner core. *Earth and Planetary Science Letters*, *228*(3), 243–253. https://doi.org/10.1016/j.epsl.2004.09.032

Dziewonski, A. M., & Anderson, D. L. (1981). Preliminary reference Earth model. *Physics of the Earth and Planetary Interiors*, *25*(4), 297–356. https://doi.org/10.1016/0031-9201(81)90046-7

Fearn, D. R., & Loper, D. E. (1981). Compositional convection and stratification of Earth's core. *Nature*, *289*(5796), 393–394. https://doi.org/10.1038/289393a0

Geballe, Z. M., Lasbleis, M., Cormier, V. F., & Day, E. A. (2013). Sharp hemisphere boundaries in a translating inner core. *Geophysical Research Letters*, *40*, 1719–1723. https://doi.org/10.1002/grl.50372

Gubbins, D. (1977). Energetics of the Earth's core. *Journal of Geophysical Research*, *43*, 453–464.

Gubbins, D., Sreenivasan, B., Mound, J., & Rost, S. (2011). Melting of the Earth's inner core. *Nature*, *473*(7347), 361–363. https://doi.org/10.1038/nature10068

Iritani, R., Takeuchi, N., & Kawakatsu, H. (2014). Intricate heterogeneous structures of the top 300km of the Earth's inner core inferred from global array data: I. Regional 1D attenuation and velocity profiles. *Physics of the Earth and Planetary Interiors*, *230*, 15–27. https://doi.org/10.1016/j.pepi.2014.02.002

Jacobs, J. A. (1953). The Earth's inner core. *Nature*, *172*(4372), 297–298. https://doi.org/10.1038/172297a0

Jeanloz, R., & Wenk, H.-R. (1988). Convection and anisotropy of the inner core. *Geophysical Research Letters*, *15*(1), 72–75. https://doi.org/10.1029/GL015i001p00072

Karato, S.-I. (1999). Seismic anisotropy of the Earth's inner core resulting from flow induced by Maxwell stresses. *Nature*, *402*(6764), 871–873. https://doi.org/10.1038/47235

Kawai, K., Takeuchi, N., & Geller, R. J. (2006). Complete synthetic seismograms up to 2 Hz for transversely isotropic spherically symmetric media. *Geophysical Journal International*, *164*(2), 411–424. https://doi.org/10.1111/j.1365246X.2005.02829.x

Li, C., van der Hilst, R. D., Engdahl, E. R., & Burdick, S. (2008). A new global model for P wave speed variations in Earth's mantle, *Geochemistry, Geophysics. Geosystems*, *9*(5). https://doi.org/10.1029/2007gc001806

Loper, D. E. (1978). The gravitationally powered dynamo. *Geophysical Journal of the Royal Astronomical Society*, *54*(2), 389–404. https://doi.org/10.1111/j.1365-246X.1978.tb04265.x

Monnereau, M., Calvet, M., Margerin, L., & Souriau, A. (2010). Lopsided growth of Earth's inner core. *Science*, *328*(5981), 1014–1017. https://doi.org/10.1126/science.1186212

Niu, F., & Wen, L. (2001). Hemispherical variations in seismic velocity at the top of the Earth's inner core. *Nature*, *410*(6832), 1081–1084. https://doi.org/10.1038/35074073

Pejić, T., Tkalčić, H., Sambridge, M., Cormier, V. F., & Benavente, R. (2017). Attenuation tomography of the upper inner core. *Journal of Geophysical Research: Solid Earth*, *122*, 3008–3032. https://doi.org/10.1002/2016jb013692

Reaman, D. M., Daehn, G. S., & Panero, W. R. (2011). Predictive mechanism for anisotropy development in the Earth's inner core. *Earth and Planetary Science Letters*, *312*(3), 437–442. https://doi.org/10.1016/j.epsl.2011.10.038

Souriau, A., & Romanowicz, B. (1996). Anisotropy in inner core attenuation: A new type of data to constrain the nature of the solid core. *Geophysical Research Letters*, *23*(1), 1–4. https://doi.org/10.1029/95gl03583

Stroujkova, A., & Cormier, V. F. (2004). Regional variations in the uppermost 100 km of the Earth's inner core. *Journal of Geophysical Research*, *109*, B10307. https://doi.org/10.1029/2004jb002976

Sun, X., & Song, X. (2008). Tomographic inversion for three-dimensional anisotropy of Earth's inner core. *Physics of the Earth and Planetary Interiors*, *167*(1), 53–70. https://doi.org/10.1016/j.pepi.2008.02.011

Tanaka, S. (2012). Depth extent of hemispherical inner core from PKP (DF) and PKP (Cdiff) for equatorial paths. *Physics of the Earth and Planetary Interiors*, *210-211*, 50–62. https://doi.org/10.1016/j.pepi.2012.08.001

Waszek, L., & Deuss, A. (2011). Distinct layering in the hemispherical seismic velocity structure of Earth's upper inner core. *Journal of Geophysical Research*, *116*, B12313. https://doi.org/10.1029/2011jb008650

Waszek, L., & Deuss, A. (2013). A low attenuation layer in the Earth's uppermost inner core. *Geophysical Journal International*, *195*(3), 2005–2015. https://doi.org/10.1093/gji/ggt368

Wen, L., & Niu, F. (2002). Seismic velocity and attenuation structures in the top of the Earth's inner core. *Journal of Geophysical Research*, *107*(B11), 2273. https://doi.org/10.1029/2001jb000170

Yu, W.-C., Su, J., Song, T.-R. A., Huang, H.-H., Mozziconacci, L., & Huang, B.-S. (2017). The inner core hemispheric boundary near 180°W. *Physics of the Earth and Planetary Interiors*, *272*, 1–16. https://doi.org/10.1016/j.pepi.2017.09.002

Yu, W.-C., & Wen, L. (2006a). Inner core attenuation anisotropy. *Earth and Planetary Science Letters*, *245*(3), 581–594. https://doi.org/10.1016/j.epsl.2006.03.043

Yu, W.-C., & Wen, L. (2006b). Seismic velocity and attenuation structures in the top 400 km of the Earth's inner core along equatorial paths. *Journal of Geophysical Research*, *111*, B07308. https://doi.org/10.1029/2005jb003995

Yu, W.-C., & Wen, L. (2007). Complex seismic anisotropy in the top of the Earth's inner core beneath Africa. *Journal of Geophysical Research*, *112*, B08304. https://doi.org/10.1029/2006jb004868